



HAL
open science

Pyrrole-tailed imidazolium surface-active monomers: aggregation properties in aqueous solution and polymerization behavior

Stéphanie Boullanger, Emmanuel Contal, Cédric Buron, Lydie Viau

► **To cite this version:**

Stéphanie Boullanger, Emmanuel Contal, Cédric Buron, Lydie Viau. Pyrrole-tailed imidazolium surface-active monomers: aggregation properties in aqueous solution and polymerization behavior. *Journal of Molecular Liquids*, 2022, 350, pp.118588. 10.1016/j.molliq.2022.118588 . hal-03552389

HAL Id: hal-03552389

<https://hal.science/hal-03552389>

Submitted on 2 Feb 2022

HAL is a multi-disciplinary open access archive for the deposit and dissemination of scientific research documents, whether they are published or not. The documents may come from teaching and research institutions in France or abroad, or from public or private research centers.

L'archive ouverte pluridisciplinaire **HAL**, est destinée au dépôt et à la diffusion de documents scientifiques de niveau recherche, publiés ou non, émanant des établissements d'enseignement et de recherche français ou étrangers, des laboratoires publics ou privés.

1 Pyrrole-tailed imidazolium surface-active monomers: aggregation 2 properties in aqueous solution and polymerization behavior

3
4 Stéphanie Boullanger,^a Emmanuel Contal,^a Cédric Buron^a and Lydie Viau^{a*}

5
6 ^a Institut UTINAM, UMR CNRS 6213, Univ. Bourgogne-Franche-Comté, Equipe Matériaux et
7 Surfaces Fonctionnels, 16 route de Gray, 25030 Besançon Cedex, France.

8
9 * To whom correspondence should be sent: E-mail: lydie.viau@univ-fcomte.fr

10 11 **Abstract**

12 Pyrrole-functionalized imidazolium surfactants PyC_nMImBr with different alkyl chain lengths
13 ($n = 8, 10, 12$) were synthesized and their aggregation properties in water were investigated
14 by tensiometry and conductimetry. These studies show that PyC_nMImBr surfactants present
15 lower critical micellar concentration than their non-functionalized analogues due to both an
16 increased hydrophobicity resulting from the extension of the alkyl chain length upon
17 incorporation of pyrrole but also to the formation of attractive π - π interactions among pyrrole
18 moieties. The areas occupied by PyC_nMImBr molecules are always higher than those of
19 C_nMImBr surfactants showing looser molecular arrangement at the air-water interface due to
20 steric hindrance of pyrrole moieties. ¹H nuclear magnetic resonance measurements have been
21 used to shed light on the structure of the aggregates formed. In all cases, pyrrole is located
22 inside the micellar core but for the shortest alkyl chain length it tends to intercalate between
23 the alkyl chains. Micelles obtained with PyC₁₂MImBr were further used as nano-reactor to
24 prepare water-stable polypyrrole nanoparticles. For this, we conduct the chemical
25 polymerization of pyrrole inside the micelles using FeCl₃ as oxidizing agent. Polymerization
26 kinetics were followed by UV-spectroscopy. Combined with Infrared (IR) and Dynamic Light
27 Scattering (DLS) measurements, we confirmed the formation of polypyrrole particles of about
28 4 nm that were water-stable thanks to the presence of cationic imidazolium functions on their
29 surface.

30 31 **Keywords**

33 **1. Introduction**

34 Intrinsically conducting polymers (ICPs) have found a lot of applications like in sensors,[1]
35 anticorrosion coatings,[2] energy storage[3] and optical devices.[4] Increasingly, researchers
36 are applying the knowledge gained in these areas toward biomedical applications including
37 biosensing,[5] drug delivery[6] and implantable medical devices.[7] The majority of these
38 studies have focused on the use of Polypyrrole (PPy) which is biocompatible. However, as
39 many others ICPs, PPy suffers from low solubility which renders its processability difficult.
40 Thus, one way to circumvent this solubility problem is to introduce charged side chains as in
41 polyelectrolytes. Poly(ionic liquids) (PILs), a special class of polyelectrolytes, that contain
42 functional groups derived from ionic liquids monomers (imidazolium or pyridinium cations
43 for instance)[8] have been used as steric stabilizers and as phase transfer agents of polypyrrole
44 thus allowing the transfer of PPy micrometers particles from water to a variety of organic
45 solvent.[9, 10] PILs that possess an intrinsically conducting polymers (ICP) backbone like
46 polypyrrole have been synthesized with the objective to combine ionic and electronic
47 conducting properties in the same polymers.[11] These PIL-ICP hybrids have been shown to
48 be able to disperse multi-wall carbon nanotubes in various solvents. Compared to the use of
49 classical ionic liquids (ILs), the use of PIL-ICP allows a higher wrapping of the carbon
50 nanotubes while providing additional electronic conductivities to the CNTs through the
51 polypyrrole backbone.[12]

52 Water-soluble ICPs show exceptional fluorescence quenching efficiencies in the presence of
53 oppositely charged acceptors and are of particular interest for imaging, diagnosis, and therapy
54 applications.^[13, 14] Besides that, in recent years, special attention has been paid to the
55 development of conjugated polymer nanoparticles (CPNs).[15] Indeed, CPNs possess several
56 advantages for biological imaging and sensing applications like their high brightness, large
57 extinction coefficients, superior photostability, low cytotoxicity, facile chemical synthesis and
58 tunable spectral properties. These CPNs are classically obtained *via* two methods:
59 miniemulsion and reprecipitation. Water-dispersive PPy CPNs of less than 100 nm were
60 synthesized without any template or surfactants by Liao and collaborators using 2,4-
61 diaminodiphenylamine as an initiator in aqueous solution[16] and by Gelling *et al.* using
62 ozone as oxidizing agent.[17]

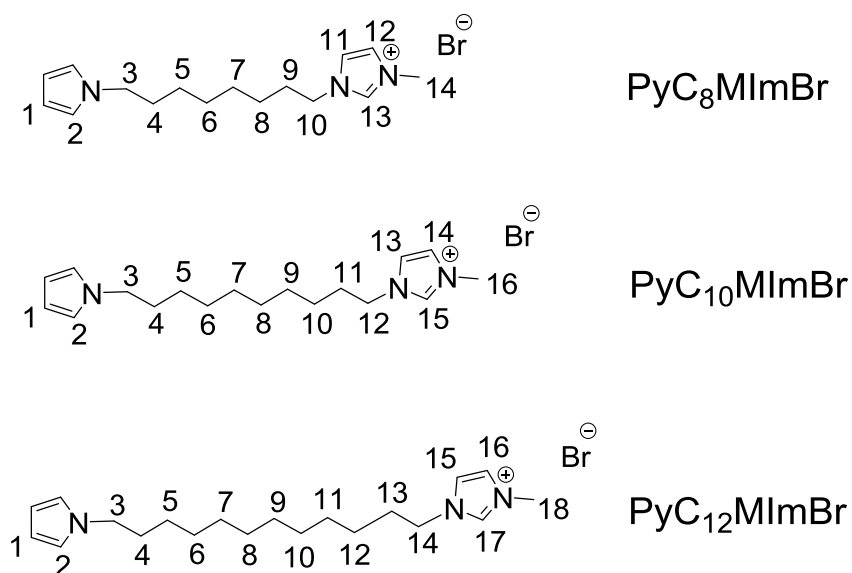
63 One other interesting alternative to elaborate water soluble CPNs would be to use surface-
64 active monomers *i.e.* surfmers like pyrrole-functionalized surfactants. To our knowledge, this
65 approach has never been reported before. However, the interfacial and micellar behaviors of
66 pyrrole-functionalized ammonium surfactants were studied and these monomers were further
67 electropolymerized to build well-organized interfacial structures.[18, 19] The surfactant
68 behavior of other pyrrole-based compounds including phosphonate-based ones, has also been
69 studied.[20] Concomitantly, imidazolium and pyridinium-based surfactants bearing a terminal
70 pyrrole group have been also used as structure-directing agent to elaborate ordered
71 mesoporous silica structure. Pyrrole units were easily polymerized *via* chemical oxidation
72 and, consequently, highly ordered hexagonal mesoporous silicas with aligned polypyrrole
73 nanowires in channels were achieved. After silica etching, aligned PPy nanowires were
74 obtained.[21] Using the same surfactant, the latter authors reported the synthesis of PPy
75 capsules with tunable thickness by simple modification of sol-gel conditions.[22] CPNs have
76 been obtained by the microemulsion polymerization method using an imidazolium-
77 functionalized pyrrole monomer containing a short butyl alkyl chain between each groups and
78 used as sensor in DNA detection.[23] Imidazolium-tailed pyrrole surfactants were more
79 recently used as fluidic light sensing materials for preparing flexible optoelectronic
80 sensors[24] and were also electrochemically polymerized to obtain polypyrrole films with
81 wrinkle structure. This latter method constitutes a way to immobilize ionic liquids on solid
82 surface[25] and can be further used for solid-phase microextraction.[26] Other examples of
83 imidazolium-based surfactants containing a polymerizable monomer include the work of
84 Firestone and co-workers on thiophene-tailed imidazolium[27] and of Zheng and
85 collaborators on carbazole-tailed imidazolium surfactants.[28]

86 This literature survey indicates that pyrrole-tailed imidazolium PyC_nMImBr molecules have
87 been used for the preparation of different materials such as polypyrrole films, porous
88 materials and PILs. Some of these studies have even taken benefit from the surfactant
89 properties of these molecules to prepare well-structured materials. However, surprisingly,
90 their surfactant behavior has not been studied in detail. Only recently, the aggregation
91 behavior and interfacial electrokinetic properties of $\text{PyC}_{12}\text{MImBr}$ were studied by dielectric
92 spectroscopy showing spontaneously formation of spherical micelles at concentration higher
93 than the Critical Micellar Concentration (CMC = 8.5 mM).[29]

94 The main objective of this paper is thus to fill this gap and to exemplify another case of the
95 use of surfactant based-ionic liquids for the elaboration of nanoparticles.[30] In the present
96 paper, surface activities and CMCs were determined by surface tension, conductimetry and

97 NMR and were compared with data obtained for long alkyl chain imidazolium bromide ILs.
 98 As these PyC_nMImBr surfactants can be considered as polymerizable surfactant *i.e.* as
 99 surfmers, we studied in the second part of this work, the polymerization ability of one of this
 100 surfmer surfactant to produce water-dispersible polymer nanospheres. The chemical structures
 101 and designations for these PyC_nMImBr surfactants are shown in Figure 1.

102



103

104 **Fig.1.** Chemical structures and labeling of the investigated PyC_nMImBr ($n = 8, 10$ and 12).

105

106 2. Experimental

107 2.1. Materials

108 The chemicals used were obtained from the following commercial sources: Pyrrole and NaH
 109 from Acros Organics[®] 1,8-dibromooctane, 1,10-dibromodecane and 1,12-dibromododecane
 110 from Alfa-Aesar[®], *N*-methylimidazole from Aldrich[®]. Dry DMF was obtained by a solvent
 111 purification system PureSolve MD5 from Innovative Technology. Preparative purifications
 112 were performed by silica gel flash column chromatography (VWR 40-63 μM). Toluene and
 113 solvents used as eluents are off technical grade.

114 2.2. Synthesis of *N*-Bromoalkyle pyrrole PyC_nBr

115

116 **General procedure.** Dibromoalkane was dissolved at 0°C in 100 mL of dry DMF. In another
 117 flask, pyrrole was added to a cooled suspension (0°C) of NaH (60%wt) in dry DMF (100
 118 mL). This mixture was allowed to reach room temperature and stirred for 30 minutes then
 119 cooled again to 0°C . The resulting solution was poured into the dibromoalkane solution by

120 canula. The mixture was allowed to reach room temperature and stirred for 24 hours. The
121 resulting solution was hydrolyzed by addition of water and the product was extracted with
122 AcOEt (3×100 mL). The resulting organic phase was washed with water (3×100 mL), dried
123 over Na₂SO₄, filtered and the solvent was removed under vacuum. The resulting compound
124 was purified by silica gel chromatography (eluent: dichloromethane/petroleum ether, 1:9).

125 **PyC₈Br**. General procedure was followed using 1,8-dibromooctane (12.16 g, 44.7 mmol, 1.5
126 equiv), pyrrole (2 g, 29.8 mmol, 1eq) and NaH (60% wt) (1.31 g, 32.7 mmol, 1.1 equiv).
127 PyC₈Br was obtained as a transparent oil (4.3 g, 56%). ¹H NMR (400 MHz, CDCl₃): δ = 6.65
128 (t, *J* = 2.1Hz, 2H, H₂), 6.14 (t, *J* = 2.1Hz, 2H, H₁), 3.87 (t, ³*J* = 7.1 Hz, 2H, H₃), 3.40 (t, ³*J* =
129 6.8 Hz, 2H, H₁₀), 1.84 (qt, ³*J* = 6.8 Hz, 2H, H₉), 1.76 (m, 2H, H₄), 1.45 (m, 2H, H₈), 1.33 (m,
130 6H, H₅, H₆, H₇). ¹³C{¹H} NMR (100.6 MHz, CDCl₃): δ = 120.5 (C2), 107.9 (C1), 49.7 (C3),
131 34.0 (C10), 32.8 (C9), 31.6 (C4), 29.1 (C6), 28.7 (C7), 28.1 (C8), 26.7 (C5) ppm. IR (ATR):
132 3100, 2927, 2854, 1541, 1499, 1459, 1358, 1279, 1256, 1087, 1060, 997, 816, 718, 644, 616,
133 560 cm⁻¹.

134 **PyC₁₀Br**. General procedure was followed using 13.41 g (44.7 mmol) of 1,10-
135 dibromodecane, 2 g of pyrrole (29.8 mmol) and NaH (60 wt%) (1.32 g, 32.8 mmol). PyC₁₀Br
136 was obtained as a transparent oil (3.13g, 37%). ¹H NMR (400 MHz, CDCl₃): δ = 6.66 (t, *J* =
137 2.1Hz, 2H, H₂), 6.15 (t, *J* = 2.1Hz, 2H, H₁), 3.87 (t, ³*J* = 7.2 Hz, 2H, H₃), 3.42 (t, ³*J* = 7.2 Hz,
138 2H, H₁₂), 1.85 (qt, ³*J* = 7.2 Hz, 2H, H₁₁), 1.77 (m, 2H, H₄), 1.43 (m, 2H, H₁₀), 1.29 (m, 10H,
139 H₅, H₆, H₇, H₈ and H₉). ¹³C{¹H} NMR (100.6 MHz, CDCl₃): δ = 120.5 (C2), 107.8 (C1), 49.7
140 (C3), 34.1 (C12), 32.9 (C11), 31.6 (C4), 29.5 (C6), 29.4 (C7), 29.3 (C8), 28.8 (C9), 28.2
141 (C10), 26.8 (C5) ppm. IR (ATR): 3100, 2924, 2853, 1499, 1462, 1357, 1280 1087, 1062, 967,
142 717, 645, 616, 560 cm⁻¹.

143 **PyC₁₂Br**. General procedure was followed using 14.67 g (44.7 mmol) of 1,12-
144 dibromododecane, 2 g of pyrrole (29.8 mmol) and NaH (60 wt%) (1.31 g, 32.7 mmol).
145 PyC₁₂Br was obtained as a transparent oil that became solid upon standing in the fridge (4.34
146 g, 46%).

147 ¹H NMR (400 MHz, CDCl₃): δ = 6.62 (t, *J* = 2.1Hz, 2H, H₂), 6.14 (t, *J* = 2.1Hz, 2H, H₁), 3.86
148 (t, ³*J* = 7.2 Hz, 2H, H₃), 3.41 (t, ³*J* = 7.2 Hz, 2H, H₁₄), 1.84 (qt, ³*J* = 7.2 Hz, 2H, H₁₃), 1.76 (m,
149 2H, H₄), 1.42 (m, 2H, H₁₂), 1.30 (m, 14H, H₅, H₆, H₇, H₈, H₉, H₁₀, H₁₁). ¹³C{¹H} NMR (100.6
150 MHz, CDCl₃): δ = 120.6 (C2), 107.8 (C1), 49.7 (C3), 34.2 (C14), 32.9 (C13), 31.8 (C4), 29.5
151 (C6, C8, C11 and C12), 29.3 (C7), 28.9 (C9), 28.3 (C10), 26.9 (C5) ppm. IR (ATR): 2923,
152 2853, 1499, 1461, 1374, 1281 1088, 1063, 967, 717, 647, 616, 560 cm⁻¹.

153

154 2.3. Synthesis of Pyrrole-functionalized imidazolium surfactants PyC_nMImBr

155 **General procedure.** PyC_nBr was dissolved in 70 mL of toluene before addition of *N*-
156 methylimidazole. The resulting mixture was reflux for 24 hours. After cooling down to room
157 temperature, two phases were formed. The lower phase that contained the product was
158 washed several times with diethyl ether (3×50 mL) and the solvent was evaporated under
159 vacuum.

160 **PyC₈MImBr.** General procedure was followed using 7.36 g (28.5 mmol) of PyC₈Br and 2.81
161 g (34.2 mmol) of *N*-methylimidazole. The final product was recovered as a creamy powder
162 (9.50 g, 98%). *m_p* = 79°C. ¹H NMR (400 MHz, CDCl₃): δ = 10.61 (s, 1H, H₁₃), 7.37 (t, ³*J* =
163 1.9 Hz, 1H, H₁₂), 7.28 (t, ³*J* = 1.9 Hz, 1H, H₁₁), 6.63 (s, 2H, H₂), 6.11 (s, 2H, H₁), 4.30 (t, ³*J* =
164 7.5 Hz, 2H, H₁₀), 4.11 (s, 3H, H₁₄), 3.85 (t, ³*J* = 7.5 Hz, 2H, H₃), 1.89 (m, 2H, H₉), 1.73 (m,
165 2H, H₄), 1.32 (m, 8H, H₅, H₆, H₇, H₈). ¹³C{¹H} NMR (100.6 MHz, CDCl₃): δ = 137.6 (C13),
166 123.6 (C12), 121.9 (C11), 120.5 (C2), 107.8 (C1), 50.1 (C10), 49.5 (C3), 36.7 (C14), 31.5
167 (C4), 30.2 (C9), 28.8 (C6/C8), 26.5 (C5), 26.1 (C7) ppm. IR (ATR): 3083, 3036, 2926, 2853,
168 1659, 1564, 1500, 1456, 1377, 1335, 1276, 1152, 1093, 970, 870, 780, 738, 659 cm⁻¹. Anal.
169 Calc for C₁₆H₂₆BrN₃ (340.30): %C 56.47, %H 7.70, %N 12.35; found %C 56.33, %H
170 7.66, %N 12.43.

171 **PyC₁₀MImBr.** General procedure was followed using 2.96 g (10.3 mmol) of PyC₁₀Br and
172 0.98 mL (12.4 mmol) of *N*-methylimidazole. PyC₁₀MImBr was obtained as a yellowish oil
173 (2.86 g, 74%). ¹H NMR (400 MHz, CDCl₃): δ = 10.66 (s, 1H, H₁₅), 7.30 (t, ³*J* = 1.9 Hz, 1H,
174 H₁₄), 7.23 (t, ³*J* = 1.9 Hz, 1H, H₁₃), 6.64 (t, ³*J* = 2.0 Hz, 2H, H₂), 6.12 (t, ³*J* = 2.0 Hz, 2H, H₁),
175 4.30 (t, ³*J* = 7.5 Hz, 2H, H₁₂), 4.12 (s, 3H, H₁₆), 3.85 (t, ³*J* = 7.5 Hz, 2H, H₃), 1.91 (m, 2H,
176 H₁₁), 1.74 (m, 2H, H₄), 1.28 (m, 12H, H₅, H₆, H₇, H₈, H₉, H₁₀). ¹³C{¹H} NMR (100.6 MHz,
177 CDCl₃): δ = 137.4 (C15), 123.6 (C14), 121.9 (C13), 120.5 (C2), 107.7 (C1), 50.1 (C12), 49.6
178 (C3), 36.7 (C16), 31.5 (C4), 30.3 (C11), 29.1 (C6/C7/C8/C9), 26.7 (C5), 26.2 (C10) ppm. IR
179 (ATR): 3136, 3057, 2924, 2852, 1567, 1500, 1460, 1370, 1278, 1167, 1089, 1062, 966, 826,
180 723, 651, 619 cm⁻¹. Anal. Calc for C₁₈H₃₀BrN₃·1.5 H₂O (395.73): %C 54.68, %H 8.41,
181 %N 10.62; found %C 54.24, %H 8.14, %N 10.63.

182

183 **PyC₁₂MImBr.** General procedure was followed using 7.11 g (22.6 mmol) of PyC₁₂Br and
184 2.23 g (27.2 mmol) of *N*-methylimidazole. PyC₁₂MImBr was obtained as a yellowish oil (8.19
185 g, 91%). ¹H NMR (400 MHz, CDCl₃): δ = 10.76 (s, 1H, H₁₇), 7.24 (t, ³*J* = 1.9 Hz, 1H, H₁₆),

186 7.20 (t, $^3J = 1.9$ Hz, 1H, H₁₅), 6.64 (t, $^3J = 2.0$ Hz, 2H, H₂), 6.12 (t, $^3J = 2.0$ Hz, 2H, H₁), 4.31
187 (t, $^3J = 7.5$ Hz, 2H, H₁₄), 4.12 (s, 3H, H₁₈), 3.85 (t, $^3J = 7.5$ Hz, 2H, H₃), 1.91 (m, 2H, H₁₃),
188 1.75 (m, 2H, H₄), 1.27 (m, 16H, H₅, H₆, H₇, H₈, H₉, H₁₀, H₁₁, H₁₂). ¹³C{¹H} NMR (100.6 MHz,
189 CDCl₃): $\delta = 137.7$ (C17), 123.5 (C16), 121.8 (C15), 120.5 (C2), 107.8 (C1), 50.3 (C14), 49.7
190 (C3), 36.9 (C18), 31.5 (C4), 30.3 (C13), 29.3 (C6/C7/C8/C9/C10/C11), 26.8 (C5), 26.3
191 (C12).ppm. IR (ATR): 3067, 2923, 2853, 1567, 1501, 1456, 1367, 1278, 1167, 1087, 965,
192 826, 723, 653, 617 cm⁻¹. Anal. Calc for C₂₀H₃₄BrN₃.1H₂O (414.42): %C 57.96, %H
193 8.75, %N 10.14; found %C 57.92, %H 8.80, %N 10.39.

194 **2.4. Synthesis of Polypyrrole nanoparticles**

195 132 mg (332 μ mol) of PyC₁₂MImBr were dissolved in 4 mL pure H₂O (C = 12 \times CMC), then
196 2.3 equivalents (220 mg) of FeCl₃.6H₂O was added and the mixture was stirred at room
197 temperature or 50°C.

198 **2.5. Physical measurements and instrumentation**

200 **Interfacial tension measurements.** Surface tension was measured using a tensiometer Krüss
201 K100 by the Wilhelmy plate method at 25°C. Each measurement was averaged over 20
202 values. Glass container and plate were cleaned with oxygen peroxide for 10 min and rinsed
203 thoroughly with distilled water. Surface tension was considered at equilibrium when the
204 standard deviation of five consecutive measurements did not exceed 0.10 mN.m⁻¹. Samples
205 have been prepared by successive dilutions with Milli-Q water and carefully homogenized.

206 **Conductimetry.** The conductivity measurements were performed using a SevenEasy
207 conductivity meter (Mettler Toledo) at 25°C. Before measuring the PyC_nMImBr solutions, the
208 probe was calibrated with a standardized 1413 μ S.cm⁻¹ standard conductivity solution (Mettler
209 Toledo). The measurements were carried out by continuous dilution of a concentrated solution
210 of PyC_nMImBr with Milli-Q water. After any dilution, the solution was stirred and
211 equilibrated for 10 min. Each experiment was repeated in duplicate. Measurements were
212 performed with an uncertainty of less than 0.5%.

213 **Infrared Spectra** were recorded with a 4 cm⁻¹ resolution on a Bruker vertex70 FTIR
214 spectrometer using a Platinum ATR accessory equipped with a diamond crystal.

215 **NMR.** The ¹H and ¹³C NMR spectra were obtained on a Bruker AVANCE 400 HD
216 instrument. ¹H chemical shifts were referenced to the proton impurity of the NMR solvent and
217 ¹³C chemical shifts to the NMR solvent.

218 **UV-visible** absorption spectra were measured on a Cary-300 spectrometer with a 300-800 nm
219 scan range, a scan rate of 600 nm.min⁻¹ and a resolution of 1 nm.

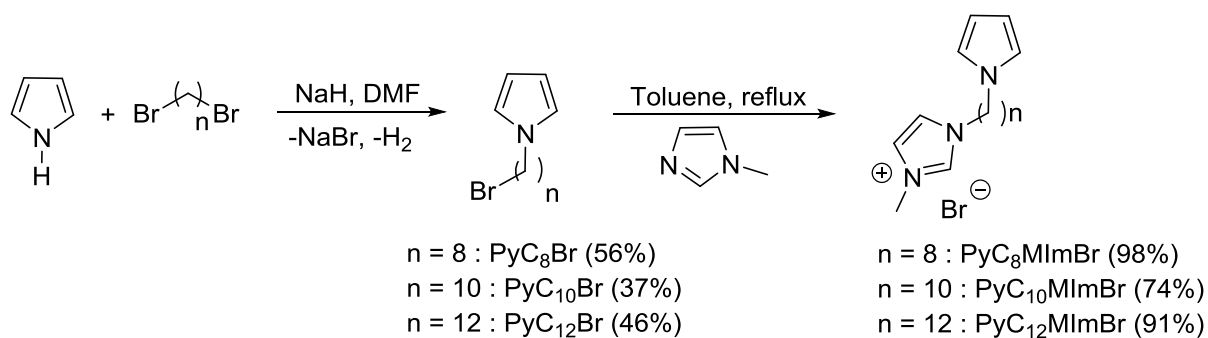
220 **The hydrodynamic sizes of the particles** were measured on a Malvern NanoZS equipped
221 with a He-Ne laser ($\lambda = 632.8$ nm) at 25°C using the back-scattered mode at an angle of 173°.
222 The correlation function of Dynamic Light Scattering (DLS) was analyzed with the general-
223 purpose method to obtain the distribution of diffusion coefficients of the solutes. The apparent
224 equivalent hydrodynamic diameters (D_h) were determined from the cumulant method using
225 the Stokes-Einstein equation. Mean diameter values were obtained from triplicate runs.

226 **Elemental analyses** were performed on a Flash EA 1112 (Thermofisher) elemental analyzer.

227 3. Results and discussion

228 3.1. Surfactants synthesis

229 Three surfactants PyC_nMImBr containing an imidazolium head and a pyrrole-functionalized
230 long alkyl chains ($n = 8, 10$ and 12) were obtained by a two steps procedure as described by
231 Zhang and collaborators for PyC₁₂MImBr.[21] The first step consists in the *N*-alkylation of
232 pyrrole by dibromoalkane in the presence of NaH. An excess of dibromoalkane was used to
233 limit the formation of the dipyrrolylalkane. This step is followed by a quaternization reaction
234 using *N*-methyl imidazole (Scheme 1). The structural characterization and the purity of the
235 final products were determined by ¹H and ¹³C NMR, IR spectroscopy and elemental analyses.
236 The ¹H NMR spectrum of PyC₈MImBr does not present any unexpected signals from
237 unremoved solvent or unreacted intermediates. Only in the case of PyC₁₀MImBr and
238 PyC₁₂MImBr, small amount of water impurity was found in the ¹H NMR spectra at 1.7 ppm.
239 The estimate values of water contents based on NMR integrals match well with those found
240 by elemental analysis. Based on these results the purity of all PyC_nMImBr final compounds
241 was estimated to be superior to 95%. (see experimental section and ESI (Figures S1-S18)).

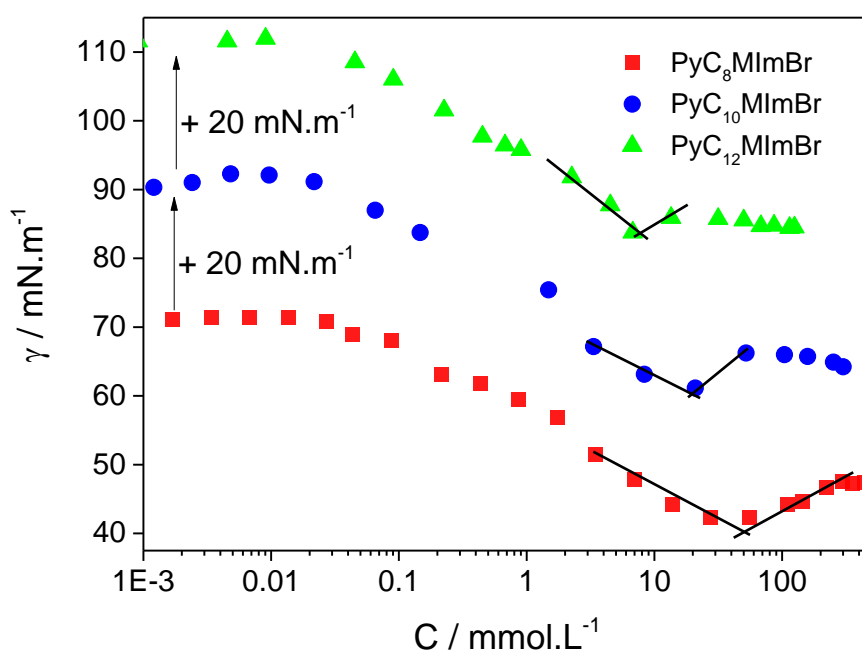


243 **Scheme 1.** Synthesis of pyrrole-tailed imidazolium surfactants PyC_nMImBr ($n = 8, 10, 12$).

244

245 3.2. Surface activity

246 The surfactant behavior of the resulting compounds has been investigated by surface tension
247 measurements. Surface tensions of the solutions *versus* PyC_nMImBr concentration in the
248 logarithmic scale are displayed in Fig. 2. A decrease in surface tension with increasing
249 PyC_nMImBr concentration is observed due to the accumulation of PyC_nMImBr at the air-
250 water surface. In all cases, a minimum of surface tension is observed that is followed by a
251 positive slope and then a plateau. As already described by Goodchild *et al.*, this observation
252 might be ascribed to the formation of surface micelles prior to aggregation leading to a
253 minimum in the area per molecule followed by the recovery of a surface monolayer for
254 concentrations greater than CMC.[31] This phenomena was already observed with other
255 functionalized-imidazolium ionic liquids.[32, 33] It should be noted that the plateau was more
256 easily reached in the following order $\text{PyC}_8\text{MImBr} < \text{PyC}_{10}\text{MImBr} < \text{PyC}_{12}\text{MImBr}$ suggesting
257 more favorable aggregation in the same order.



258

259 **Fig.2.** Surface tension isotherms of PyC_nMImBr ($n = 8, 10, 12$) aqueous solutions at 25°C .
260 For the sake of clarity, the amplitudes for $\text{PyC}_{10}\text{MImBr}$ and $\text{PyC}_{12}\text{MImBr}$ have been shifted
261 by $+20 \text{ mN.m}^{-1}$.

262 The CMCs were taken at the minimum surface tension which was considered to be the
263 aggregation onset.[34] Table 1 summarizes the CMC values determined from surface tension
264 measurements for PyC_nMImBr. Data previously obtained by other authors by tensiometry for
265 non-functionalized imidazolium surfactants (C_nMImBr) are also included for comparison. As
266 classically observed for conventional cationic imidazolium surfactants, the CMC decreases
267 with an increase of the alkyl chain length.[35] Even though the data reported for C_nMImBr
268 differ from one to the others, it is clear that PyC_nMImBr compounds have slightly lower
269 CMCs than their parent C_nMImBr analogues. Zheng and collaborators reported the self-
270 aggregation of carbazole-tailed imidazolium compounds (CarbazoleC_nMImBr) in aqueous
271 solutions and found even much lower CMCs (CMC = 0.712 mM for CarbazoleC₁₀MImBr vs
272 21 mM for PyC₁₀MImBr and CMC = 0.188 mM for CarbazoleC₁₂MImBr vs 8 mM for
273 PyC₁₂MImBr).[28] As in the case of carbazole-tailed imidazolium compounds, the lower
274 CMC values found for our pyrrole-tailed compounds compared to non-functionalized
275 imidazolium ones can be attributed to an increased hydrophobicity resulting from the
276 extension of the alkyl chain length upon incorporation of pyrrole but also to the formation of
277 attractive π - π interactions among pyrrole moieties. As such, our pyrrole-functionalized
278 surfactants present higher CMC values compared to carbazole ones due to weaker π - π
279 interaction among pyrrole moieties and to the lower hydrophobicity of pyrrole compared to
280 carbazole.

281 The CMC value of PyC₁₂MImBr can also be compared to the one obtained for a
282 dodecyltrimethyl ammonium bromide surfactant containing a pyrrole moiety at the end of the
283 hydrocarbon tail for which a CMC value of 13 mM was determined.[19] In this later case, the
284 CMC is slightly higher than the one of our PyC₁₂MImBr compound due to the presence of a
285 trimethylammonium head group. Indeed, this head group is known to lead to higher CMC
286 values compared to imidazolium ones for which the positive charges are delocalized on the
287 imidazolium ring.[36] The CMC value for PyC₁₂MImBr is also in good agreement with the
288 one reported by Zhao and collaborator (CMC = 8.5 mM) determined by dielectric
289 spectroscopy.[29]

290 The ability to decrease surface tension was characterized by two other parameters:

291
292 - The efficiency of adsorption pC₂₀ defined as the negative logarithm of the
293 amphiphilic molecule's concentration required to reduce the surface tension of the
294 pure solvent by 20 mN.m⁻¹ (Eq 1)

$$295 \quad pC_{20} = -\log C_{20} \quad (1)$$

296 - The effectiveness of the surface tension reduction π_{CMC} defined as equation (2):

297
$$\pi_{\text{CMC}} = \gamma_0 - \gamma_{\text{CMC}} \quad (2)$$

298 where γ_0 is the surface tension of pure water and γ_{CMC} the surface tension of the solution at the
299 CMC.

300 pC_{20} values increased with the alkyl chain length, which confirmed a higher efficiency of
301 surfactant activity upon increasing n . In our series, a slightly lower value of pC_{20} is obtained
302 for PyC₈MImBr while the values are very close for PyC₁₀MImBr and PyC₁₂MImBr.
303 Comparison of the PyC _{n} MImBr series with the C _{n} MImBr one shows that the pC_{20} value of
304 PyC₁₀MImBr is higher than its C₁₀MImBr counterpart while pC_{20} values for PyC₁₂MImBr and
305 C₁₂MImBr are nearly identical. Thus, even in the absence of data for C₈MImBr, it can be
306 concluded that PyC₈MImBr and PyC₁₀MImBr have higher adsorption efficiency than
307 C₈MImBr and C₁₀MImBr while PyC₁₂MImBr has only moderate higher efficiency than
308 C₁₂MImBr. π_{CMC} varies only slightly with increasing the alkyl chain length.

309 The area occupied by a surfactant molecule at the air–water interface A_{min} was calculated
310 according to equation (3):

311
$$A_{\text{min}} = \frac{1}{N_A \Gamma_{\text{max}}} \quad (3)$$

312 Where N_A is the Avogadro constant ($6.022 \times 10^{23} \text{ mol}^{-1}$), Γ_{max} is the surface excess
313 concentration calculated by applying the Gibbs equation (4) for monocationic surfactant[37]:

314
$$\Gamma_{\text{max}} = -\frac{1}{2RT} \left(\frac{\partial \gamma}{\partial \ln C} \right)_T \quad (4)$$

315 Where R is the gas constant ($8.314 \text{ J} \cdot \text{K}^{-1} \cdot \text{mol}^{-1}$), T is the absolute temperature and $\frac{\partial \gamma}{\partial \ln C}$ is the
316 slope of the surface tension γ vs $\ln C$ dependence when the concentration is near the CMC.

317

318 Recent reports have pointed serious limitations in applying the Gibbs equation accurately to
319 determine surface excess Γ_{max} of cationic surfactants.[38] Indeed, it has been shown that
320 adsorption increases through and above the CMC rendering the polynomial fitting of surface
321 tension unreliable. As such, methods such as neutron reflection that do not require
322 concentrations or activities to determine surface excess would be preferable. Another point
323 that has been pointed out by the same authors is that Wilhelmy plate methods might also lead
324 to incomplete wetting. The exact values of surface areas reported here should thus be taken

325 with caution. However, it seems to us that comparison of data obtained by the same method
 326 for different compounds gives a correct tendency.

327 As can be seen in Table 1, the A_{\min} value is the highest for PyC₈MImBr ($A_{\min} = 171 \text{ \AA}^2$) and
 328 then decreases for PyC₁₀MImBr and PyC₁₂MImBr ($A_{\min} = 141$ and 129 \AA^2 , respectively) due
 329 to closer packing of the monomer at the air/water interface upon increasing the alkyl chain
 330 length. This more efficient packing is due to an increase of van der Waals forces between
 331 alkyl chains. The areas occupied by PyC_{*n*}MImBr molecules are always higher than those of
 332 C_{*n*}MImBr surfactants showing looser molecular arrangement at the air-water interface due to
 333 steric hindrance of pyrrole moieties. The observation of higher surface areas compared to
 334 classical imidazolium ionic liquids is also in accordance with the results of Dong and
 335 collaborators for carbazole-tailed imidazolium ionic liquids ($A_{\min} = 191$ and 193 \AA^2 for $n = 10$
 336 and 12 , respectively). However, as expected from the smaller size of pyrrole compared to
 337 carbazole, our surface areas are smaller.[28]

338 **Table 1.** Surface properties at 25°C for PyC_{*n*}MImBr and C_{*n*}MImBr compounds.

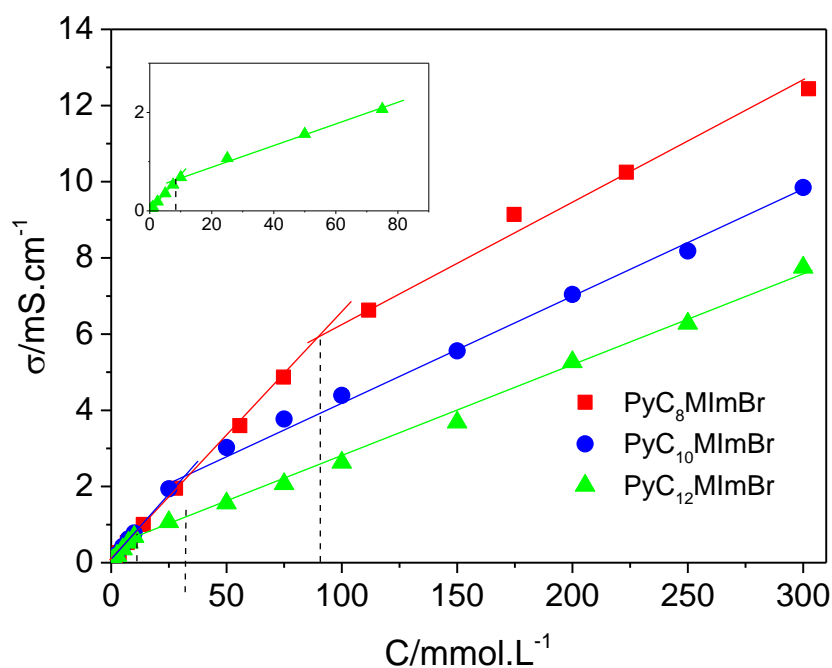
Compounds	CMC (mM)	pC ₂₀	π_{CMC} (mN.m ⁻¹)	A_{\min} (\AA^2)	Γ_{\max} ($\mu\text{mol.m}^{-2}$)
PyC ₈ MImBr	50 ± 5	2.46	29.7	171	0.965
PyC ₁₀ MImBr	20 ± 2	2.65	31.0	141	1.24
PyC ₁₂ MImBr	8 ± 1	2.69	31.0	129	1.28
C ₈ MImBr	170[39], 150[31], 121[40]	-	-	124[39], 60[31]	-
C ₁₀ MImBr	33[39], 40[31], 29.3[41], 20[40]	2.15[41]	33.3[41]	91[39], 48[31], 96.7[41]	1.72[41]
C ₁₂ MImBr	9[39], 10.9[41], 4.3[40]	2.67[41]	33.6[41]	67[39], 86.8[41]	1.91[41]

339

340 3.3 Conductivity measurements

341 Variation of specific conductance of aqueous solutions of PyC_{*n*}MImBr as a function of
 342 concentration is shown in Figure 3. Two linear regimes in the concentration dependence of
 343 the conductivity are clearly observed with a second slope lower than the first one due to the
 344 decrease of free charged species in the bulk. The slope break was assigned to the onset of the

345 CMC. Data obtained by this method are collected in Table 2 and data previously reported for
 346 C_n MImBr are also included for comparison. The CMCs values are consistent with the values
 347 obtained by surface tension measurements for the longest alkyl chain lengths ($n = 10$ and 12)
 348 but differ in the case of PyC₈MImBr (see table 3). This might be attributed to the presence of
 349 the above-mentioned minimum in surface tension measurements. In the case of PyC₈MImBr,
 350 this minimum was relatively broad and might have led to some errors in the determination of
 351 the CMC. Thus, it is anticipated that conductivity measurements give a more accurate value
 352 of the CMC for the shortest chain homologues. In the PyC _{n} MImBr series, the degree of
 353 ionization α determined by Frahm's method *i.e.* as the ratio of the slopes of the linear
 354 fragments above and below CMC[42] decreases with the increase of the alkyl chain length
 355 from $n = 8$ to $n = 10$ and then remains constant with further increase of n . This observation is
 356 in line with the observation of constant values of π_{CMC} and pC_{20} for PyC₁₀MImBr and
 357 PyC₁₂MImBr (see discussion above).



358
 359 **Fig.3.** Variation of conductivities vs concentrations of PyC _{n} MImBr ($n = 8, 10, 12$) aqueous
 360 solutions at 25°C.

361 **Table 2.** CMCs of PyC _{n} MImBr determined at 25°C by conductimetry with the corresponding
 362 degree of ionization and free energy of aggregation.

Compounds	CMC (mM)	α	ΔG_m^0 (kJ.mol ⁻¹)
-----------	----------	----------	--

PyC ₈ MImBr	87	0.43	-25.2
PyC ₁₀ MImBr	29	0.34	-30.9
PyC ₁₂ MImBr	7.7	0.34	-36.4
C ₈ MImBr	160[39], 150[31]	0.57[39]	-20.7[39], -23.5[36]
C ₁₀ MImBr	42[39], 40[31], 41[36], 32.9[41]	0.33[39], 0.29[36], 0.31[41]	-29.7[39], -29.6[36]
C ₁₂ MImBr	10[39], 9.8[36], 8.5[41]	0.26[39], 0.27[36], 0.27[41]	-37.2[39], -37.2[36]

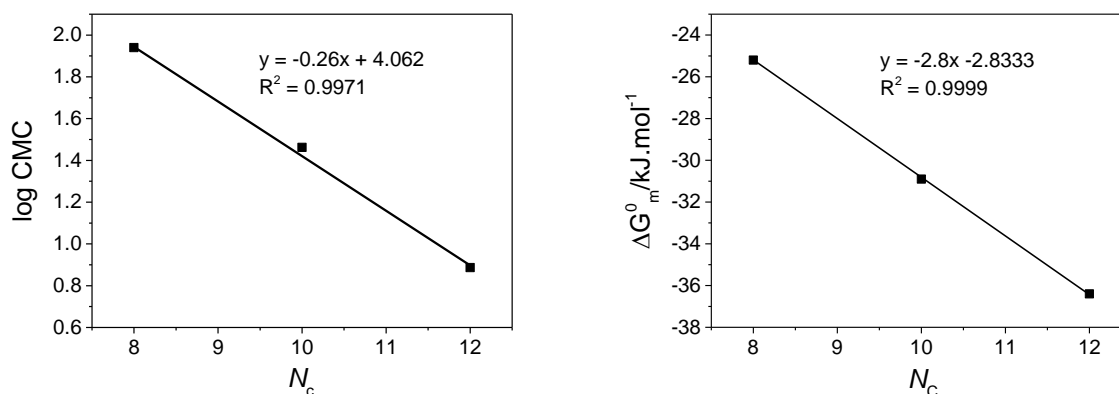
363

364 Based on CMCs values determined by conductimetry, we plotted the logarithm variation of
 365 CMC (in mmol.L⁻¹) against the number of carbons in the alkyl chain length (N_c) (Figure 4
 366 left). This plot follows the Stauff-Klevens rule[43] given by equation (5):

$$367 \quad \log(\text{CMC}) = A - B \times N_c \quad (5)$$

368 where A and B are constant for a homologous series of surfactants.

369 The slope B of this linear variation is -0.26, a value slightly higher than what was reported for
 370 C_nMImBr (-0.28)[44] but also higher than the value reported for CarbazoleC_nMImBr
 371 compounds (-0.23).[28] As this slope is a measure of the effect of each methylene groups on
 372 the CMC it shows that the presence of a pyrrole moiety alters the effect of the methylene
 373 group on the CMC compared to non-functionalized C_nMImBr surfactants but this effect is less
 374 marked than in the presence of a carbazole unit.



375 **Fig. 4.** Logarithm of CMC (mM) (left) and ΔG_m^0 (right) as a function of the number of carbon
 376 atoms N_c for PyC_nMImBr at 25°C.

377

378 The pseudo-phase model of micellization was applied to determine the Gibbs energy of
 379 aggregation (ΔG_m^0) according to the following equation:[37]

380

$$\Delta G_m^0 = (2 - \alpha)RT \ln \chi_{CMC} \quad (6)$$

382
383 where χ_{CMC} is the critical micellar concentration expressed in mole fraction, α is the degree of
384 ionization.

385 The obtained ΔG_m^0 values are reported in Table 2. Negative values of ΔG_m^0 indicate the
386 spontaneity of the micellization process and ΔG_m^0 becomes more negative with an increase in
387 the alkyl chain length/hydrophobicity. As previously reported, ΔG_m^0 could be divided into
388 contributions from the head group $\Delta G_{m, \text{head group}}^0$, the methylene group of the hydrophobic
389 chain $\Delta G_{m, \text{CH}_2}^0$ and the terminal group of the alkyl chain $\Delta G_{m, \text{terminal}}^0$ (equation 7).[45] These
390 contributions express the fact that aggregates form under the influence of both attractive and
391 repulsive forces. Attractive forces are associated with the poor solubility of alkyl chains,
392 while effective repulsive forces result from the high solubility of head groups.

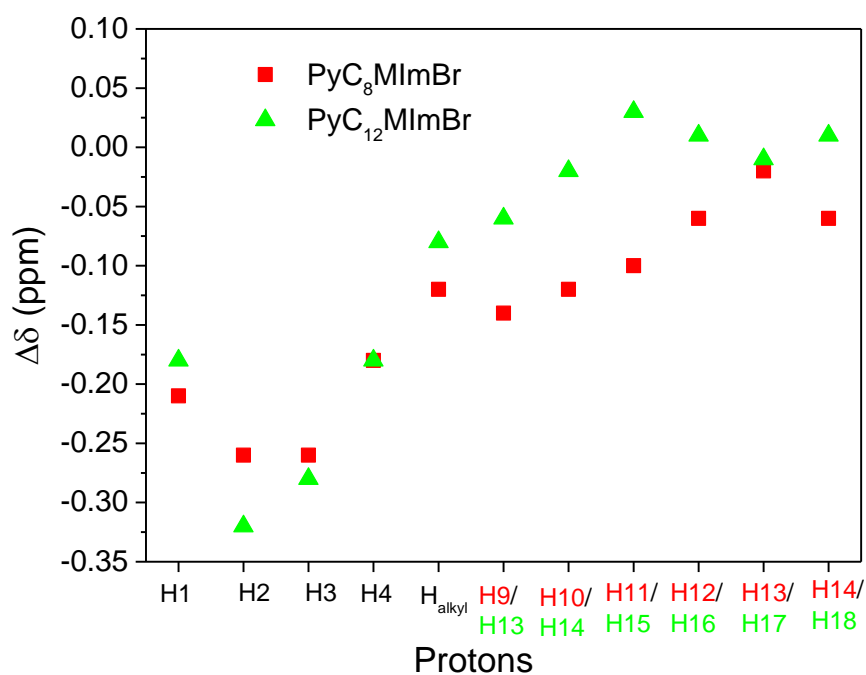
$$\Delta G_m^0 = \Delta G_{m, \text{head group}}^0 + \Delta G_{m, \text{terminal}}^0 + N_c \Delta G_{m, \text{CH}_2}^0 \quad (7)$$

394 The plot of ΔG_m^0 versus $n\text{CH}_2$ (N_c) is presented in Figure 4 (right). It gives a straight line with
395 an intercept equal to $\Delta G_{m, \text{head group}}^0 + \Delta G_{m, \text{terminal}}^0$ and a slope equal to $\Delta G_{m, \text{CH}_2}^0$. Data obtained
396 for PyC_nMImBr were compared to those reported by Wang *et al.* for C_nMImBr.[45] The
397 $\Delta G_{m, \text{CH}_2}^0$ values are close ($\Delta G_{m, \text{CH}_2}^0 = -2.80 \text{ kJ.mol}^{-1}$ for PyC_nMImBr and $-2.96 \text{ kJ.mol}^{-1}$ for
398 C_nMImBr). However, for PyC_nMImBr the $\Delta G_{m, \text{head group}}^0 + \Delta G_{m, \text{terminal}}^0$ term is higher than
399 for C_nMImBr ($-2.83 \text{ kJ.mol}^{-1}$ and $-3.77 \text{ kJ.mol}^{-1}$, respectively). As the two series are
400 composed of the same imidazolium head group and the same anion, this difference might be
401 attributed to the presence of a pyrrole group which is less hydrophobic than the methyl group
402 in C_nMImBr.

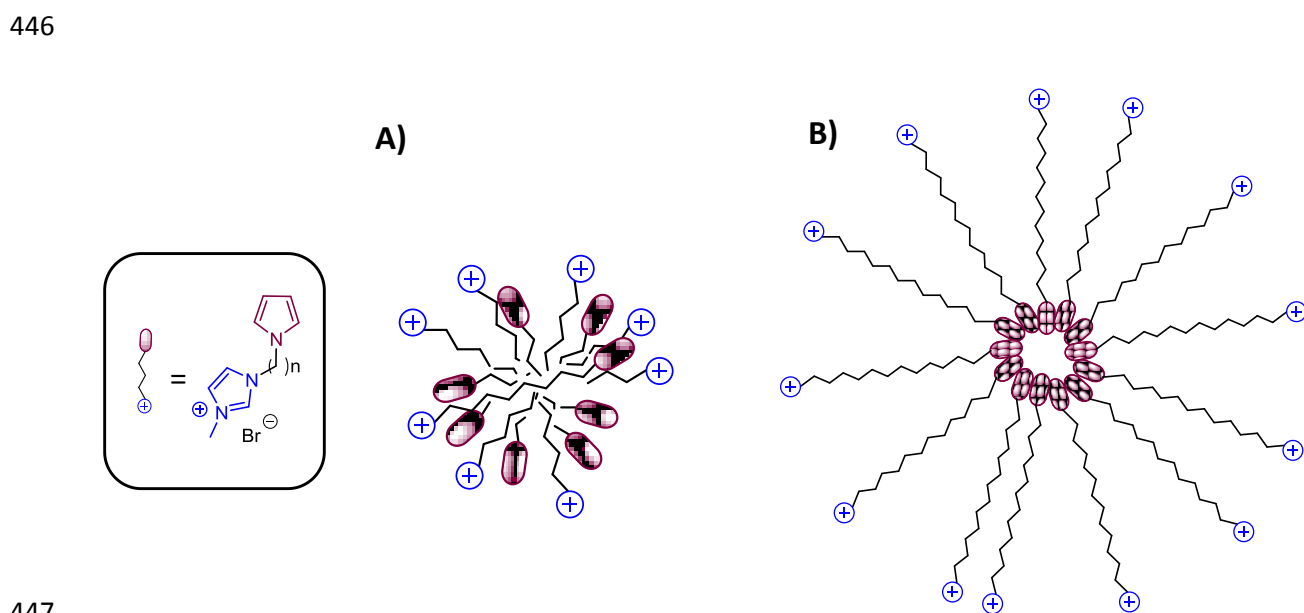
403 3.3. ¹H NMR spectra

404 The ¹H NMR spectra of the compounds with the shortest alkyl chain length (PyC₈MImBr)
405 and the longest alkyl chain length (PyC₁₂MImBr) were registered in D₂O at different
406 concentrations (Figure S19 and S21). For all concentrations considered in this work, the
407 chemical shifts δ_{obs} for the different protons of PyC_nMImBr are summarized in Supporting
408 Information (Tables S1 and S2). The difference $\Delta\delta$ obtained for different protons between the
409 chemical shifts measured at the highest concentration δ_{max} and those obtained at the lowest
410 concentration δ_{min} are shown in Figure 5. All protons of PyC₈MImBr move upfield ($\Delta\delta < 0$)
411 and the shift is much more important for the protons of the pyrrole ring (H1 and H2) or close
412 to it (H3 and H4) (see Figure 1 for protons attribution). In this latter case also, there is a

413 pseudo linear variation of the chemical shift for the protons of the alkyl chain between the
414 pyrrole and the imidazolium rings. The alkyl protons close to the pyrrole ring (H3 and H4)
415 undergo the more important upfield shift and this shift decreases as the protons are located
416 further away from the pyrrole ring. For PyC₁₂MImBr, the protons of the pyrrole moiety and
417 close to it move also upfield. However, the protons of the CH₂ close to the imidazolium ring
418 (H13 and H14) and those of the imidazolium ring (H15-H17) do not shift significantly.
419 For surfactants bearing only a classical alkyl chain, a downfield shift off the ¹H NMR
420 chemical signals is commonly observed for the protons of the alkyl chains upon aggregation
421 due to a polarity decrease when going from the aqueous phase to the micellar core.[46] Other
422 studies have demonstrated that, for surfactants with aromatic counteranions for instance, upon
423 incorporation of these aromatic anions into surfactant micelles, two additional effects are
424 observed. Aromatic protons move upfield upon intercalation into the micelles. Additionally,
425 protons of the alkyl chain of the surfactant in the proximity of the shielding cone of the
426 aromatic ring move upfield. As only the protons located in the field of the ring are shifted, it
427 is possible to provide information on the location of the aromatic ring.[47] The upfield shift of
428 the pyrrole protons thus evidences that the pyrrole is located inside the micellar core. On the
429 other hand, the upfield shift of the protons of the alkyl chain shows that the pyrrole
430 intercalates between the alkyl chain resulting in their upfield shift. The determination of the
431 exact location of the pyrrole ring within the alkyl chains is, in our case difficult, as many
432 protons of the alkyl chain are not discernible one from the others. For PyC₈MImBr, all
433 protons of the alkyl chains undergo the shielding effect meaning that they are all located close
434 to pyrrole moieties. For PyC₁₂MImBr, protons of the alkyl chains undergo low shielding
435 meaning that they are not in close proximity to the pyrrole ring. At the same time, the $\Delta\delta$
436 value for H2 of the pyrrole ring is higher for PyC₁₂MImBr than for PyC₈MImBr ($\Delta\delta = -0.32$
437 and -0.26 for PyC₁₂MImBr and PyC₈MImBr respectively) showing that it is more deeply
438 incorporated into the micelles. Based on these results, a schematic illustration of the proposed
439 structures of micelles formed by pyrrole-alkyl-imidazolium surfactants is presented in Figure
440 6.
441
442



443
 444 **Fig. 5.** Amplitude of variation of chemical shifts $\Delta\delta$ for various protons for PyC₈MImBr and
 445 PyC₁₂MImBr in D₂O at 25 °C.



447
 448 **Fig. 6.** Schematic representation of the proposed structures of micelles formed with A)
 449 PyC₈MImBr and B) PyC₁₂MImBr.

450
 451 It has been shown that ¹H NMR chemical shifts can be used to determine the CMC of
 452 surfactants. [48] Under fast exchange occurring on the NMR time scale, the observed

453 chemical shift for a corresponding proton is a weight average of the monomer (δ_{mono}) and
454 micelle (δ_{mic}) chemical shifts which can be expressed as equation (7):

455

$$456 \quad \delta_{obs} = \delta_{mon} \left(\frac{C_{mon}}{C} \right) + \delta_{mic} \left(\frac{C_{mic}}{C} \right) \quad (7)$$

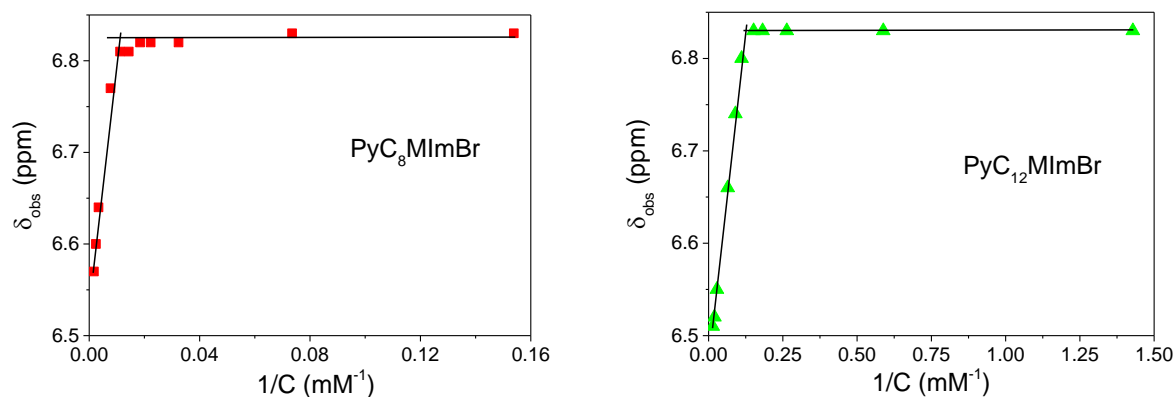
457 Where C_{mon} , C_{mic} and C are the concentrations of surfactant monomers, surfactant in micelles
458 and total surfactants in solution, respectively. Above the CMC, it is assumed that the free
459 monomer concentration remains constant so that $C_{mic} = C - CMC$. Inserting this relation in
460 equation (7) gives equation (8):

461

$$462 \quad \delta_{obs} = \delta_{mic} - \left(\frac{CMC}{C} \right) (\delta_{mic} - \delta_{mon}) \quad (8)$$

463 According to equation 8, the plots of δ_{obs} versus $1/C$ should give two straight lines with their
464 intersection corresponding to CMC.

465 Figure 7 shows the variation of δ_{obs} of the H2 protons of the pyrrole ring versus $1/C$ for
466 PyC_8MImBr and $PyC_{12}MImBr$ (see figure 1 for protons attribution). As expected, two straight
467 lines are obtained in each case and CMCs values determined from these plots are summarized
468 in table 3. These values are in good agreement with those obtained by conductimetry. Note
469 that same results were obtained considering other protons (Figures S20 and S22).



470 **Fig. 7.** Chemical shift δ_{obs} as a function of $1/C$ for H2 for PyC_8MImBr (left) and $PyC_{12}MImBr$
471 (right) at 25°C

472

473

474 **Table 3.** CMCs (mM) values of PyC_nMImBr as determined from different methods at 25°C.

Compounds	¹ H NMR	Surface tension	Conductimetry
PyC ₈ MImBr	89	50 ± 5	87
PyC ₁₀ MImBr	nd	20 ± 2	29
PyC ₁₂ MImBr	8	8 ± 1	7.1

475

476

477 3.4. Polymerization

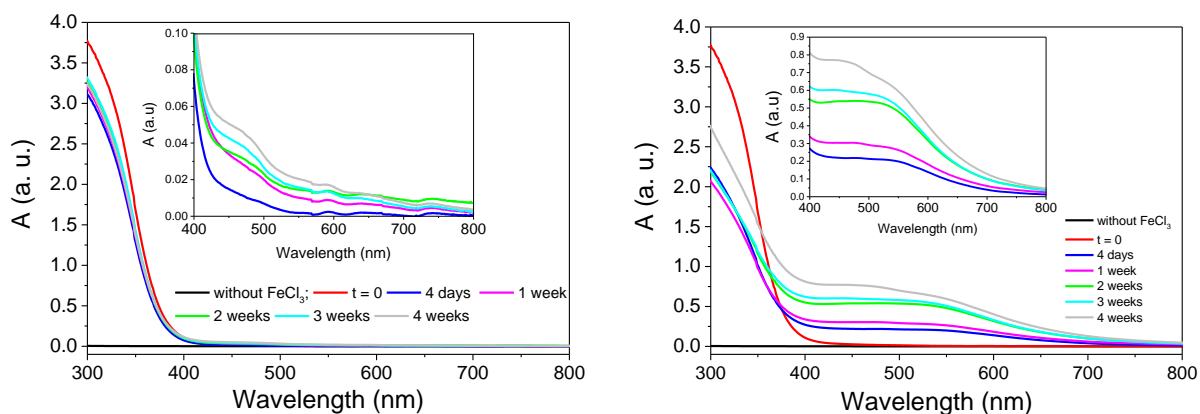
478 The chemical polymerization of pyrrole inside micelles was reported by Zhang and
 479 collaborators using FeCl₃ as oxidizing agent. Micelles were obtained by the self-assembly of
 480 different cationic surfactants used as template (cetyltrimethylammonium bromide (CTAB) or
 481 dodecyltrimethylammonium bromide (DTAB)). Polypyrrole-sphere like nanostructures with
 482 diameters ranging from 35 to 70 nm were obtained. [49]

483 In order to generate water-stable polypyrrole particles, we tested our ionic surfactants as
 484 functional surface-active monomers (surfmers). We focus our study on PyC₁₂MImBr which
 485 acts as better surfactant (lower CMC). We thus performed the chemical polymerization of
 486 PyC₁₂MImBr in the same conditions as Zhang and collaborators, using a concentration equal
 487 to 12 times the CMC and FeCl₃ as the oxidant (2.3 eq). Polymerization reactions were
 488 performed at room temperature and 50°C and kinetics were followed by UV-visible
 489 spectroscopy.

490 As can be seen on figure 8, the monomer PyC₁₂MImBr does not absorb between 300 and 800
 491 nm (black curve). After addition of FeCl₃ (red curve) a strong band at 300 nm is clearly
 492 observed due to the absorption of FeCl₃. [50] After 4 days, a band at about 480 nm is observed
 493 characteristic to the formation of polypyrrole. This spectrum is in accordance with the one
 494 obtained for polypyrrole nanospheres reported by Vetter *et al.* [17] The intensity of this band
 495 slightly increases with time but the process is quite slow since the absorbance increases
 496 slightly during 4 weeks. As can be seen from the picture on figure 9, the sample presents a
 497 brown colour characteristic to the formation of polypyrrole.

498 In order to improve the polymerization kinetics, the same experiments were then realized at
 499 50°C, a temperature at which the micelles were found to be stable (Figure 9). As the same
 500 concentrations were used at room temperature and 50°C, the intensity of the absorption bands

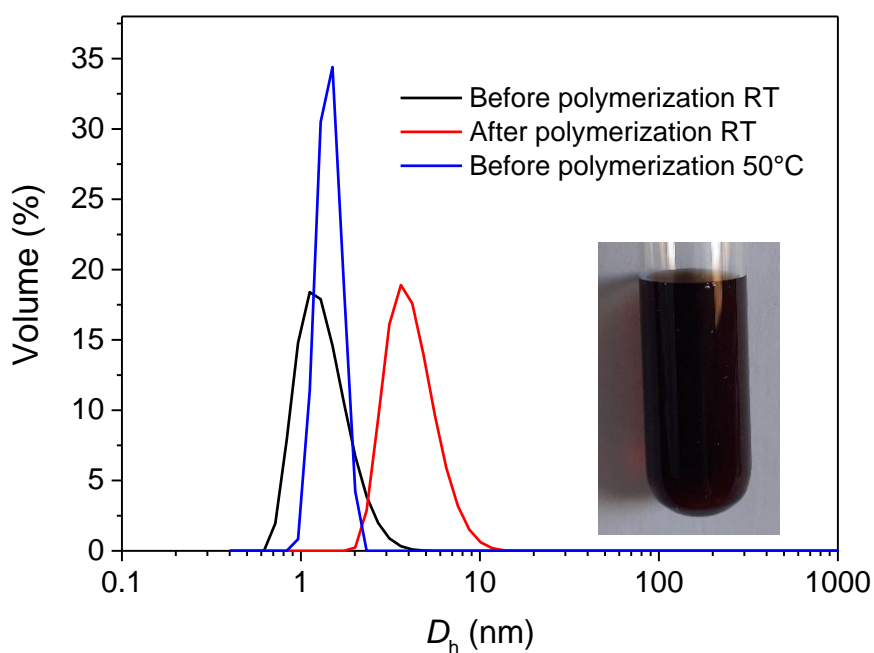
501 can be compared between the two experiments. Clearly, the band at 480 nm is much more
 502 intense when the reaction is performed at 50°C meaning that the kinetic of the polymerization
 503 was increased upon heating[51] and that the amount of polypyrrole formed was more
 504 important. This band extends also up to 550 nm due to partial oxidative doping of the
 505 polypyrrole.[50, 52]



506
 507 **Fig. 8.** UV-Visible spectra recorded during polymerization of PyC₁₂MImBr (C= 12× CMC) at
 508 room temperature (left) and 50°C (right) with corresponding pictures of the solutions obtained
 509 at the end of polymerization.

510 Figure 9 presents the aggregates size distribution before and after polymerization performed
 511 at room temperature. Before polymerization, the PyC₁₂MImBr solution is composed of
 512 micelles with a hydrodynamic diameter D_h of 1.4 ± 0.5 nm about twice the length of one
 513 surfactant. Note that the same distribution was obtained even after several weeks meaning that
 514 micelles were stable for weeks. After 4 weeks of polymerization at room temperature,
 515 micelles were still present, but with an average diameter $D_h = 4.3 \pm 1.5$ nm. Micelles swelled
 516 because the pyrrole moieties take more space in the core of micelles when they are
 517 polymerized. Thus, the surfactants chains were disturbed in their packing and finally the
 518 micelles were bigger. The inset in Figure 9 illustrates the water-stability of the resulting
 519 polypyrrole nanoparticles.

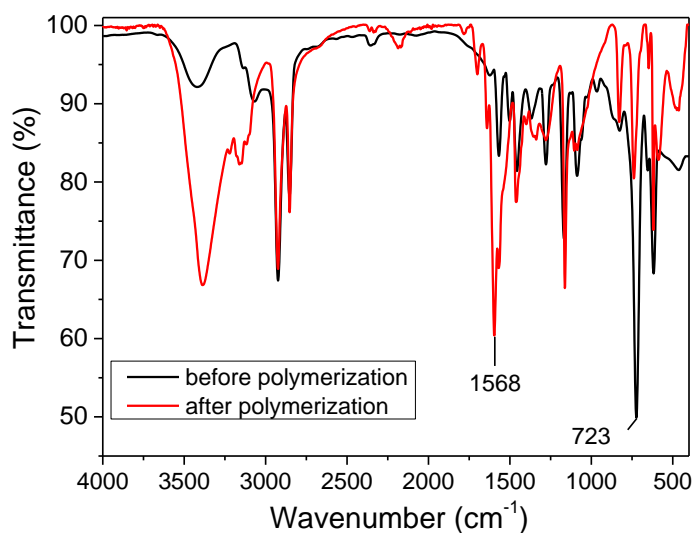
520 Even though the kinetic was increased at 50°C, DLS measurements obtained in this case
 521 evidenced multimodal distributions (results not shown). Thus, uniform size particles of
 522 polypyrrole could not be obtained under this condition.



523

524 **Fig. 9.** Size distribution of polypyrrole particles obtained from DLS at 25 °C and 50°C of
 525 PyC₁₂MImBr before polymerization (black curve) and after polymerization at room
 526 temperature (red). The inset shows photographs illustrating the stability of the polypyrrole
 527 particles in water.

528 After polymerization, the sample obtained after 4 weeks at room temperature was lyophilized
 529 to register its IR spectrum. Figure 10 disclosed a comparison of the IR spectra of
 530 PyC₁₂MImBr before and after polymerization.



531 **Fig. 10.** FT-IR spectra of PyC₁₂MImBr before and after polymerization.

532 Even though clear attribution of the IR bands is difficult due to an overlapping of the band's
533 characteristics of polypyrrole and those of the imidazolium group, it is clearly observed that
534 after polymerization, the intensity of the peaks at 1568 cm⁻¹ increases while, concomitantly,
535 the intensity of the peak at 723 cm⁻¹ decreases. The band at 1568 cm⁻¹ can be ascribed to the
536 C=C stretching vibration of polypyrrole.[53] As the peak at 723 cm⁻¹ is attributed to the α (C-
537 H) bending mode of the pyrrole ring, its significant decrease indicates that α - α coupling of
538 the pyrrole units occurred thus confirming the formation of polypyrrole.[54] Note that similar
539 IR spectra were obtained by Li and collaborators when using PyC₁₂MImBr to prepare ordered
540 silica with polypyrrole in the channels.[21]

541 **4. Conclusion**

542 The surfactant properties of pyrrole-functionalized imidazolium ionic liquids were studied by
543 different techniques. Compared with their non-functionalized analogues, they present lower
544 CMCs and higher adsorption efficiency as expected from the lengthening of the alkyl chain
545 length and the presence of π - π interactions among adjacent pyrrole moieties. However, we
546 also observed a deviation of the evolution of ΔG_m^0 values with the number of CH₂ groups in
547 the alkyl chain from what was obtained with classical imidazolium surfactants. Indeed, the
548 contribution of $\Delta G_{m, \text{terminal}}^0$ in the case of the pyrrole end group is lower than for the methyl
549 group due to its lower hydrophobicity. Additional ¹H NMR experiments have shown that
550 pyrrole is located inside the micellar cores and, in the case of PyC₈MImBr, it intercalates
551 between the alkyl chains.

552 The chemical polymerization of pyrrole using PyC₁₂MImBr as surfmer was performed both at
553 room temperature and at 50°C. At room temperature, the polymerization is low but results in
554 the formation of polypyrrole nanoparticles with hydrodynamic diameters D_h of about 4 nm.
555 The stabilization of these particles is ensured by electrostatic repulsions between the
556 imidazolium moieties on their surface. Even though the polymerization kinetic of pyrrole
557 inside the micelles can be accelerate at higher temperature, it does not allow the formation of
558 monodisperse polypyrrole particles.

559 In this study, we thus develop an easy and simple to implement method to prepare water-
560 stable polypyrrole nanoparticles using ionic liquids-based surfactants. These nanoparticles
561 might find applications as interlayers of organic light emitting diodes (OLEDs), antistatic
562 coatings and as inkjet-printed chemical sensors.

563

564 **Acknowledgements**

565 The authors would like to thank the OSU Theta for its financial support.

566

567 **References**

568

569 [1] M. Ates, A review study of (bio)sensor systems based on conducting polymers, *Mater.*
570 *Sci. Eng., C*, 33 (2013) 1853-1859.

571 [2] D. Aradilla, D. Azambuja, F. Estrany, J.I. Iribarren, C.A. Ferreira, C. Alemán, Poly(3,4-
572 ethylenedioxythiophene) on self-assembled alkanethiol monolayers for corrosion protection,
573 *Polym. Chem.*, 2 (2011) 2548-2556.

574 [3] G.A. Snook, P. Kao, A.S. Best, Conducting-polymer-based supercapacitor devices and
575 electrodes, *J. Power Sources*, 196 (2011) 1-12.

576 [4] A.O. Patil, A.J. Heeger, F. Wudl, Optical properties of conducting polymers, *Chem. Rev.*,
577 88 (1988) 183-200.

578 [5] W.-K. Oh, O.S. Kwon, J. Jang, Conducting Polymer Nanomaterials for Biomedical
579 Applications: Cellular Interfacing and Biosensing, *Polym. Rev.*, 53 (2013) 407-442.

580 [6] D. Svirskis, J. Travas-Sejdic, A. Rodgers, S. Garg, Electrochemically controlled drug
581 delivery based on intrinsically conducting polymers, *J. Controlled Release*, 146 (2010) 6-15.

582 [7] P.M. George, A.W. Lyckman, D.A. LaVan, A. Hegde, Y. Leung, R. Avasare, C. Testa,
583 P.M. Alexander, R. Langer, M. Sur, Fabrication and biocompatibility of polypyrrole implants
584 suitable for neural prosthetics, *Biomaterials*, 26 (2005) 3511-3519.

585 [8] J. Yuan, M. Antonietti, Poly(ionic liquid)s: Polymers expanding classical property
586 profiles, *Polymer*, 52 (2011) 1469-1482.

587 [9] R. Marcilla, C. Pozo-Gonzalo, J. Rodríguez, J.A. Alduncin, J.A. Pomposo, D. Mecerreyes,
588 Use of polymeric ionic liquids as stabilizers in the synthesis of polypyrrole organic
589 dispersions, *Synth. Met.*, 156 (2006) 1133-1138.

590 [10] W. Qian, J. Texter, F. Yan, *Frontiers in poly(ionic liquid)s: syntheses and applications*,
591 *Chem. Soc. Rev.*, 46 (2017) 1124-1159.

592 [11] D. Mecerreyes, Polymeric ionic liquids: Broadening the properties and applications of
593 polyelectrolytes, *Prog. Polym. Sci.*, 36 (2011) 1629-1648.

594 [12] P. Chatterjee, E.M. Nofen, W.W. Xu, C. Hom, H.Q. Jiang, L.L. Dai, Pyrrole-based
595 poly(ionic liquids) as efficient stabilizers for formation of hollow multi-walled carbon
596 nanotubes particles, *J. Colloid Interface Sci.*, 504 (2017) 140-148.

597 [13] J. Wang, D. Wang, E.K. Miller, D. Moses, G.C. Bazan, A.J. Heeger, Photoluminescence
598 of Water-Soluble Conjugated Polymers: Origin of Enhanced Quenching by Charge Transfer,
599 *Macromolecules*, 33 (2000) 5153-5158.

600 [14] C. Zhu, L. Liu, Q. Yang, F. Lv, S. Wang, Water-Soluble Conjugated Polymers for
601 Imaging, Diagnosis, and Therapy, *Chem. Rev.*, 112 (2012) 4687-4735.

602 [15] J. Pecher, S. Mecking, Nanoparticles of Conjugated Polymers, *Chem. Rev.*, 110 (2010)
603 6260-6279.

604 [16] Y.Z. Liao, X.G. Li, R.B. Kaner, Facile Synthesis of Water-Dispersible Conducting
605 Polymer Nanospheres, *ACS Nano*, 4 (2010) 5193-5202.

606 [17] C.A. Vetter, A. Suryawanshi, J.R. Lamb, B. Law, V.J. Gelling, Novel Synthesis of Stable
607 Polypyrrole Nanospheres Using Ozone, *Langmuir*, 27 (2011) 13719-13728.

608 [18] I. Berlot, P. Labbe, J.C. Moutet, Adsorption and electrochemical oxidation on carbon of
609 micelle-forming cationic surfactants derived from pyrrole, *Langmuir*, 16 (2000) 5814-5819.

610 [19] I. Berlot, Y. Chevalier, P. Labbe, J.C. Moutet, Interfacial and micellar behavior of
611 pyrrole-containing cationic surfactants, *Langmuir*, 17 (2001) 2639-2646.

612 [20] S. Oberoi, Y. Lu, G. Busch, E. Jaehne, A. Pich, H.J.P. Adler, Novel modified pyrrole
613 monomers, 2: Behaviour in water solutions, *Des. Monomers Polym.*, 11 (2008) 69-82.

614 [21] W. Zhang, J. Cui, C. Lin, Y. Wu, L. Ma, Y. Wen, G. Li, Pyrrole containing ionic liquid
615 as tecton for construction of ordered mesoporous silica with aligned polypyrrole nanowires in
616 channels, *J. Mater. Chem.*, 19 (2009) 3962-3970.

617 [22] C. Lin, W. Zhu, H. Yang, Q. An, C.-a. Tao, W. Li, J. Cui, Z. Li, G. Li, Facile Fabrication
618 of Stimuli-Responsive Polymer Capsules with Gated Pores and Tunable Shell Thickness and
619 Composite, *Angew. Chem. Int. Ed.*, 50 (2011) 4947-4951.

620 [23] J. Zhao, F. Yan, Z. Chen, H. Diao, F. Chu, S. Yu, J. Lu, Microemulsion Polymerization
621 of Cationic Pyrroles Bearing an Imidazolium-Ionic Liquid Moiety, *J. Polym. Sci., Part A:
622 Polym. Chem.*, 47 (2009) 746-753.

623 [24] Y. He, X.-Q. Xu, S. Lv, H. Liao, Y. Wang, Dark Ionic Liquid for Flexible
624 Optoelectronics, *Langmuir*, 35 (2019) 1192-1198.

625 [25] W. Zhang, Y. Li, C. Lin, Q. An, C. Tao, Y. Gao, G. Li, Electrochemical polymerization
626 of imidazolium-ionic liquids bearing a pyrrole moiety, *J. Polym. Sci., Part A: Polym. Chem.*,
627 46 (2008) 4151-4161.

628 [26] A.M. Devasurendra, C. Zhang, J.A. Young, L.M.V. Tillekeratne, J.L. Anderson, J.R.
629 Kirchhoff, Electropolymerized Pyrrole-Based Conductive Polymeric Ionic Liquids and Their
630 Application for Solid-Phase Microextraction, *ACS Appl. Mater. Interfaces*, 9 (2017) 24955-
631 24963.

632 [27] C.T. Burns, S. Lee, S. Seifert, M.A. Firestone, Thiophene-based ionic liquids: synthesis,
633 physical properties, self-assembly, and oxidative polymerization, *Polym. Adv. Technol.*, 19
634 (2008) 1369-1382.

635 [28] B. Dong, Y.a. Gao, Y. Su, L. Zheng, J. Xu, T. Inoue, Self-Aggregation Behavior of
636 Fluorescent Carbazole-Tailed Imidazolium Ionic Liquids in Aqueous Solutions, *J. Phys.
637 Chem. B*, 114 (2010) 340-348.

638 [29] X. Fan, K. Zhao, Aggregation behavior and electrical properties of amphiphilic pyrrole-
639 tailed ionic liquids in water, from the viewpoint of dielectric relaxation spectroscopy, *Soft
640 Matter*, 10 (2014) 3259-3270.

641 [30] O.A. El Seoud, N. Keppeler, N.I. Malek, P.D. Galgano, Ionic Liquid-Based Surfactants:
642 Recent Advances in Their Syntheses, Solution Properties, and Applications, *Polymers*, 13
643 (2021) 1100.

644 [31] I. Goodchild, L. Collier, S.L. Millar, I. Prokeš, J.C.D. Lord, C.P. Butts, J. Bowers, J.R.P.
645 Webster, R.K. Heenan, Structural studies of the phase, aggregation and surface behaviour of
646 1-alkyl-3-methylimidazolium halide + water mixtures, *J. Colloid Interface Sci.*, 307 (2007)
647 455-468.

648 [32] M.T. Garcia, I. Ribosa, L. Perez, A. Manresa, F. Comelles, Aggregation Behavior and
649 Antimicrobial Activity of Ester-Functionalized Imidazolium- and Pyridinium-Based Ionic
650 Liquids in Aqueous Solution, *Langmuir*, 29 (2013) 2536-2545.

651 [33] M.T. Garcia, I. Ribosa, L. Perez, A. Manresa, F. Comelles, Self-assembly and
652 antimicrobial activity of long-chain amide-functionalized ionic liquids in aqueous solution,
653 *Colloids Surf., B*, 123 (2014) 318-325.

654 [34] A. Modaressi, H. Sifaoui, M. Mielcarz, U. Domańska, M. Rogalski, Influence of the
655 molecular structure on the aggregation of imidazolium ionic liquids in aqueous solutions,
656 *Colloids Surf., A*, 302 (2007) 181-185.

657 [35] J. Łuczak, J. Hupka, J. Thöming, C. Jungnickel, Self-organization of imidazolium ionic
658 liquids in aqueous solution, *Colloids Surf., A*, 329 (2008) 125-133.

659 [36] W.L. Zhang, Y.X. Wang, X.Y. Lan, Y. Huo, Imidazolium-based ionic liquids as
660 electrolyte additives for high-voltage Li-ion batteries, *Res. Chem. Intermed.*, 46 (2020) 3007-
661 3023.

662 [37] M. J. Rosen, *Surfactant and Interfacial Phenomena*, Wiley-Intersciences, John Wiley &
663 Sons, New Jersey, 2004, 2004.

664 [38] P.X. Li, R.K. Thomas, J. Penfold, Limitations in the Use of Surface Tension and the
665 Gibbs Equation To Determine Surface Excesses of Cationic Surfactants, *Langmuir*, 30 (2014)
666 6739-6747.

667 [39] A. Cornellas, L. Perez, F. Comelles, I. Ribosa, A. Manresa, M.T. Garcia, Self-
668 aggregation and antimicrobial activity of imidazolium and pyridinium based ionic liquids in
669 aqueous solution, *J. Colloid Interface Sci.*, 355 (2011) 164-171.

670 [40] Q.Q. Baltazar, J. Chandawalla, K. Sawyer, J.L. Anderson, Interfacial and micellar
671 properties of imidazolium-based monocationic and dicationic ionic liquids, *Colloids Surf., A*,
672 302 (2007) 150-156.

673 [41] B. Dong, N. Li, L. Zheng, L. Yu, T. Inoue, Surface Adsorption and Micelle Formation of
674 Surface Active Ionic Liquids in Aqueous Solution, *Langmuir*, 23 (2007) 4178-4182.

675 [42] J. Frahm, S. Diekmann, A. Haase, Electrostatic Properties of Ionic Micelles in Aqueous
676 Solutions, *Ber. Bunsen-Ges. Phys. Chem*, 84 (1980) 566-571.

677 [43] J. Stauff, Equilibria between molecular dissolved and colloidal substances in aqueous
678 soap dissolution. 1. Chapter: Hydrolysis of fatty acid salts, *Z. Phys. Chem. A*, 183 (1938) 55.

679 [44] T. Inoue, H. Ebina, B. Dong, L. Zheng, Electrical conductivity study on micelle
680 formation of long-chain imidazolium ionic liquids in aqueous solution, *J. Colloid Interface*
681 *Sci.*, 314 (2007) 236-241.

682 [45] J. Wang, H. Wang, S. Zhang, H. Zhang, Y. Zhao, Conductivities, Volumes,
683 Fluorescence, and Aggregation Behavior of Ionic Liquids [C₄mim][BF₄] and [C_nmim]Br (n
684 = 4, 6, 8, 10, 12) in Aqueous Solutions, *J. Phys. Chem. B*, 111 (2007) 6181-6188.

685 [46] T. Singh, A. Kumar, Aggregation Behavior of Ionic Liquids in Aqueous Solutions:
686 Effect of Alkyl Chain Length, Cations, and Anions, *The Journal of Physical Chemistry B*, 111
687 (2007) 7843-7851.

688 [47] W. Ge, H. Shi, Y. Talmon, D.J. Hart, J.L. Zakin, Synergistic Effects of Mixed Aromatic
689 Counterions on Nanostructures and Drag Reducing Effectiveness of Aqueous Cationic
690 Surfactant Solutions, *The Journal of Physical Chemistry B*, 115 (2011) 5939-5946.

691 [48] C. Chachaty, Applications of NMR methods to the physical chemistry of micellar
692 solutions, *Prog. Nucl. Magn. Reson. Spectrosc.*, 19 (1987) 183-222.

693 [49] X. Zhang, J. Zhang, W. Song, Z. Liu, Controllable Synthesis of Conducting Polypyrrole
694 Nanostructures, *The Journal of Physical Chemistry B*, 110 (2006) 1158-1165.

695 [50] B.L. Langsdorf, B.J. MacLean, J.E. Halfyard, J.A. Hughes, P.G. Pickup, Partitioning and
696 Polymerization of Pyrrole into Perfluorosulfonic Acid (Nafion) Membranes, *The Journal of*
697 *Physical Chemistry B*, 107 (2003) 2480-2484.

698 [51] C.C. Bof Bufon, J. Vollmer, T. Heinzel, P. Espindola, H. John, J. Heinze, Relationship
699 between Chain Length, Disorder, and Resistivity in Polypyrrole Films, *The Journal of*
700 *Physical Chemistry B*, 109 (2005) 19191-19199.

701 [52] G. Zotti, S. Martina, G. Wegner, A.-D. Schlüter, Well-defined pyrrole oligomers:
702 Electrochemical and UV/vis studies, *Advanced Materials*, 4 (1992) 798-801.

703 [53] M. Omastová, M. Trchová, J. Kovářová, J. Stejskal, Synthesis and structural study of
704 polypyrroles prepared in the presence of surfactants, *Synth. Met.*, 138 (2003) 447-455.

705 [54] Y. Chen, C.T. Imrie, K.S. Ryder, Pyrrole- and polypyrrole-based liquid crystals, *J.*
706 *Mater. Chem.*, 11 (2001) 990-995.

707